SRTTU

JCARME
ISSN: 2228-7922

Journal of Computational and Applied Research
in Mechanical Engineering
Vol. 4, No. 2, pp. 145- 154, Spring 2015
http://jcarme.srttu.edu

# Numerical simulation of laser beam welding of Ti6Al4V sheet

**M. Azizpour, M. Ghoreishi* and A. Khorram**

*Department of Mechanical Eng. K. N. Toosi University of Technology, Tehran, Iran*

Received: 17/08/2013
Accepted: 16/08/2014
Online: 03/03/2015

**Keywords:**
Numerical simulation,
$CO_2$ laser welding,
Ti6Al4V alloy.

**Abstract**

This paper was aimed to report the 3D finite element analysis simulation of laser welding process of Ti6Al4V 1.7 mm sheets in butt joint in order to predict the temperature distribution, hardness, and weld geometry. The butt-joint welds were made using $CO_2$ laser with the maximum power of 2.2 kW in the continuous wave mode. A part of the experimental work was carried out to verify the weld geometry with specific weld parameters including power, speed, and focal position. Another part investigated the effect of focal position on the weld bead geometry. Subsequently, the shapes of the molten pool were predicted by the numerical analysis method and compared with the results obtained through the experimentation, which led to finding a good agreement.

## 1. Introduction

Laser welding is an important joining technique which has been increasingly used in industrial manufacturing. The advantages of laser welding over convectional welding technology include low heat input, high welding speed, small heat affected zone (HAZ), and low distortion rate. These advantageous are related to high power density of laser welding. The laser welding input parameters determine the shape of laser weld bead. Weld quality strongly depends on the weld bead geometry; hence, the weld bead geometry plays an important role in determining the mechanical properties of the weld joints. Therefore, selecting the welding process parameters is crucial for obtaining the desired weld bead geometry [1].

Laser welding of Ti6Al4V is used in numerous areas, such as aerospace industries and medical device industry. The most commonly used titanium alloy is Ti6Al4V which is widely used in aerospace industries, nuclear engineering, civil industries, chemical industries, and medically implanted materials due to high stiffness strength to weigh ratio, high corrosion resistance, and biocompatibility [2].

With the increasing use of laser welding and development of computer calculating methods, there will be more dependence on using numerical simulations with finite element method (FEM) to predict the weld bead geometry.

P. Sathiya et al. [1] evaluated the weld bead geometry in the laser welding of 904 L super austenitic stainless steel using the Taguchi approach as a statistical design of experiment (DOE) technique to optimize the selected welding parameters including beam power, travel speed, and focal position.

*Corresponding author
*Email address: ghoreishi@kntu.ac.ir*

N. Siva Shanmugam et al. [3] applied finite element method (FEM) using ANSYS code to predicate the weld bead geometry of AISI 304 stainless steel in spot welding process. The varied input parameters were beam power, incident angle of the beam, and beam exposure time. K.Y. Benyounis et al. [4] studied the effect of speed, laser power, and focal position on the heat input and the weld bead geometry of laser butt welding of medium carbon steel using the response surface methodology (RSM).
Ming-Huei Yu and Yi-Chun Liao's [5] research indicated the effects of laser energy and incident angle on the pulse laser welding of stainless steel by comparing the cross-section of welds. Hanbin Du et al. [6] presented a mathematical model for flow simulation of full penetration laser beam welding, predicting the geometry profile of the titanium weld alloy.
Abdulkarieem S. Aloraier and Suraj Joshi [7] simulated the flux cored arc welding (FCAW) in single bead on plate weld of steel (AS 1548-7-460R) using finite element code SYSWELD and predicted the temperature distribution and residual stress. They compared the cross-section of the macrograph with the molten pool.
Siva Shanmugam and G. Buvanashekaran [8] predicted the bead geometry in laser welding with 1.6 mm thick AISI304 stainless steel sheets. The bead shape of T-joint laser welds was investigated by means of finite element code SYSWELD and the effects of laser beam power, welding speed, and beam incident angle were studied on the weld bead geometry.
The key for the successful analysis of the FE welding method consists of modeling several metallurgical and mechanical phenomena occurring simultaneously within the structure being welded. Fig. 1 shows the coupling mechanism among these processes. Some authors [9, 10] have shown that several simplifications are acceptable in welding simulation with minimal loss in accuracy.
It has been proved that one of the most important aspects of welding processes is the introduction of metallurgical transformation into the simulation [11-14] and an employment of coupled thermo-metallurgical analysis for the simultaneous calculation of temperature field. Moreover, phase fraction is crucial; however, no research has been carried out thoroughly for simulating the weld profile of the laser weld for Ti6Al4V considering the coupled thermo-metallurgical approach and materials with both phase- and temperature-dependent properties.
The aim of this study was to predict weld geometry and temperature distribution in the butt join laser welding process of Ti6Al4V 1.7 mm sheets. Moreover, the effect of focal position on the weld bead geometry was investigated and the results were compared with the experimental results.

## 2. Experimental work

A Ti6Al4V sheet with the chemical composition presented in Table 1 was used as the work piece material. The size of each sample was 85 mm long× 35 mm wide with the thickness of 1.7 mm. The laser welding process was done using a $CO_2$ laser (Optimo; Optima Industries, Inc.) with maximum power of 2.2 kW in the continuous wave mode and two different speeds of 13.34 and $40\frac{mm}{s}$. Argon gas with the constant pressure of 0.1 bar was used as a shielding gas. The experimental work was discussed in detail in [15].
At the simulation stage, ambient temperature was assumed to be $20^{o}C$ (initial temperature). Values of thermal conductivity, specific heat capacity, thermal expansion coefficient, and Young's modulus with the relation of temperature in two phases (α and α+β) were taken into consideration. Density of 4420 $kg/mm^3$ , Poisson's ratio of 0.33, and Steffen Boltzmann ($5.67x10^{-8}\frac{W}{m^2K}$) coefficient were considered independent from temperature. [16].

## 3. Finite element analysis

A 3D finite element model was used to simulate the laser welding process by the FE code SYSWELD. The developed model was used to predict the temperature distribution and weld geometry of 1.7 mm thick Ti6Al4V titanium alloy sheet.

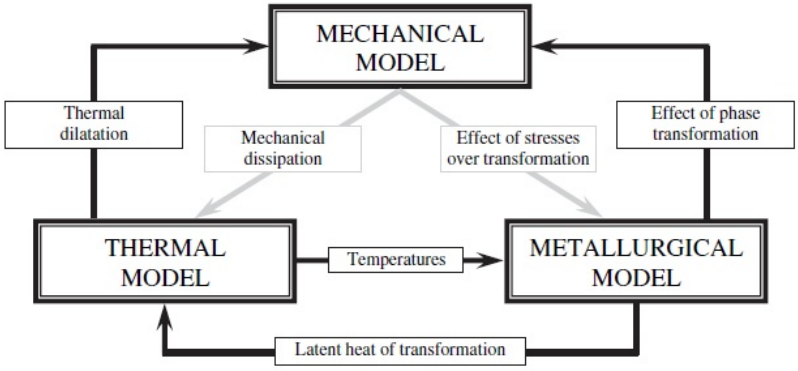


**Fig. 1.** Coupling mechanism of thermo-metallo-mechanical model.[11]

### *3.1. Finite element model*

The 3D elements were used to mesh the basic body structure representing the parent metal and weld bead. Moreover, quadrilateral elements were used to mesh all the domains representing the surfaces which were exposed to air for considering heat losses. Since in the laser modeling welding, mesh density is an important aspect, especially in HAZ, a dense mesh was used in the area close to the weld line, increasing in size toward the edges of the parent material to reduce the solution time, as shown in Fig. 2, which was mainly due to the very small size of the keyhole and HAZ in the laser welding process.
In this model, geometries with 4 -6 and 8 elements in the thickness were conducted and it turned out that using 4 elements would minimize the solution time as well as achieving the best convergence. Later, all the meshes were stuck together to ensure avoiding any non-positive stiffness matrix error.

**Table 1.** Chemical composition of Ti6Al4V.

| Element | Aluminum | Vanadium | Titanium |
|---|---|---|---|
| Percentage(Wt%) | 6 % | 3.98% | 90.02% |

### *3. 2. Heat source fitting*

The most important aspect for simulating welding process is to accurately model the welding heat source. Using heat source fitting (HSF) tool available within SYSWELD, users could calibrate a more refined heat source by adjusting the parameters to perform a steady-state thermal analysis. The steady-state computation option used in the heat source-fitting tool can be efficiently used to simulate 3D temperature fields and phase transformations.

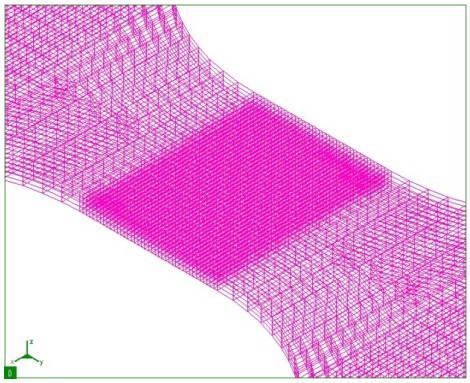

**Fig. 2.** Finite element model.

Several standard heat sources for different types of welding are available in HSF. The heat input distribution would determine the size and shape of the weld pool.
It has been found [17-19] that the best heat source model for simulating the keyhole in laser welding is conical Gaussian distribution; since this analysis is concerned with laser welding, this model was selected. The heat source start position in the model can be seen in Fig. 3.
The Gaussian distribution of heat flux may be written as [2]:

$$Q_v(r,z) = Q_0 \exp(\frac{-3r^2}{r_0^2}) \quad (1)$$

where $Q_0$ is maximum heat intensity, $r_0$ is distribution parameter, and $r$ is current radius. Height of the conical Gaussian heat source is $H = Z_e - Z_i$. $Z_e$ and $Z_i$ is the upper and lower $z$ coordinates of the cone, as shown in Fig. 4. The $r_0$ parameter is decreased linearly from the top to bottom surfaces resulting in the conical shape of the heat distribution which can be written as:

$$r_0(z) = r_e - (r_e - r_i) - \frac{z_e - z}{z_e - z_i} \quad (2)$$

And r is given as:

$$r = (x^2 + y^2)^{\frac{1}{2}} \quad (3)$$

Estimated values for $1600^0 C$ Gaussian heat source model in millimeter can be obtained as: $r_i = 0.3$ , $r_e = 0.6$ , $z_i = 1$ and $z_e = 1.65$ .

During the laser welding, a part of the energy is lost before being absorbed in the material of the work piece. For the butt-joint laser welding, it is observed that the energy loss is the 30% of the nominal power of the heat source. Accordingly, the absorbed energy is considered to be 70% of the laser power [17].

It has been also observed that 70% of laser power, 25 and 75% of heat power source are absorbed by the surface of the work piece ($Q_{surf}$) and by the keyhole wall ($Q_{bottom}$), respectively [20].

Assuming that laser beam maintains a constant $TEM_{00}$ mode, Gaussian heat flux distribution can be expressed as:

$$Q(x,y) = q_m \exp(-\frac{3(x^2 + y^2)}{R^2}) \quad (4)$$

where $q_m$ is the maximum heat flux area and R is the radius of the heat source calculated by the focal length of the focusing lens by the formula written as:

$$R = \frac{2M_0^2 \lambda f}{\pi D_0} \quad (5)$$

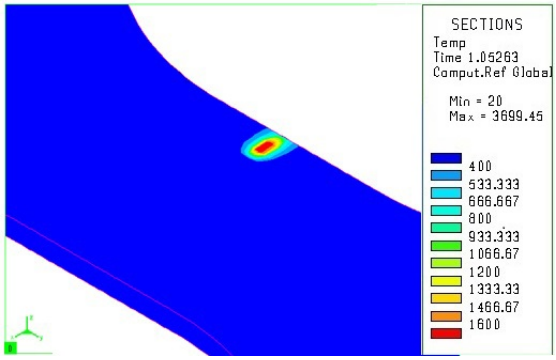


**Fig. 3.** Heat source starting position.

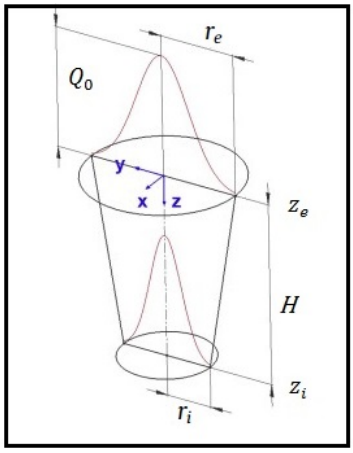


**Fig. 4.** 3D conical Gaussian distribution.

In this formula $M_0^2$ is the beam quality, f is the focal length of the focusing length and $D_0$ is the minimum diameter of the laser beam. $q_m$ can be expressed as [11]:

$$q_m = \frac{3}{\pi R^2} Q_{surf} \quad (6)$$

Assuming that the keyhole has a conical shape the Gaussian distribution of heat flux is written as [2]:

$$Q(z) = \frac{2Q_{buttom}}{\pi r_0^2 H} e^{1-(\frac{r}{r_0})^2} (1 - \frac{z}{H}) \quad (7)$$

where $r_0$ is the initial radius at top, H is the plate thickness, and r is the current radius. The summation of surface and volume heat source gives the total heat input to the model as:

$$Q_v = Q(x,y) + Q(z) \quad (8)$$

The source intensity $Q_v$ is calculated and applied to the FE model using HSF module available in SYSWELD software.

### 3. 3. Heat conduction

The following three-dimensional heat conduction equation was considered to model the heat transfer in laser transmission welding process that defined the temperature distribution within the body based on the energy conservation law, balancing the rate of the internally generated heat within the body's capacity to store this heat. Rate of thermal conduction to the boundaries can be represented as [21]:

$$\frac{\partial}{\partial x}(k_x\frac{\partial T}{\partial x})+\frac{\partial}{\partial y}(k_y\frac{\partial T}{\partial y})+\frac{\partial}{\partial z}(k_z\frac{\partial T}{\partial z})+ Q(x,y,z)=\rho c\frac{\partial T}{\partial t} \quad (9)$$

where, $k_x$,$k_y$ and $k_z$ are the thermal conductivity in the x, y and z directions (W/m-K), C is the specific heat capacity (J/kg-K), ρ is the density (kg/m3), t is the time (s), and Q(x,y,z,t) is internal heat generation rate per unit volume (W/m3).

In the laser welding process, the work piece exchanges heat with the surrounding due to convection and radiation. The surface, exposed to air, transfers the energy by the convective heat transfer mode. These surfaces are represented by domains in the model, as shown in Fig. 5.

This convective heat loss $q_{conv}$ can be expressed as:

$$q_{conv}=Ah(T_s-T_x) \quad (10)$$

where, h is convection heat transfer coefficient ($25\frac{W}{m^2K}$), $T_s$ is surface temperature, and $T_\infty$ is ambient temperature ($25^0C$).

Thermal radiation is energy emitted by matter, as a result of electromagnetic waves and it is considerable when the temperature difference between the surface and medium is high. The radiant heat loss, $q_{rad}$ , from the top surface of the work piece can be expressed as:

$$q_{rad}=\sigma\varepsilon(T_s^4-T_x^4) \quad (11)$$

Where, σ is Stefan Boltzmann constant ($5.67\text{x}10^{-8}\frac{W}{m^2K}$ ), and ε is the emissivity (0.19). The emissivity of a material (usually written ε or e) is the relative ability of its surface to emit energy by radiation.

### 3. 4. Finite element equations for heat transfer

According to Fourier's law the components of heat flow can be expressed as following and it can be put in the Eq. (15):

$$q_x=-k_x(\frac{\partial T}{\partial x}) \quad (12)$$

$$q_y=-k_y(\frac{\partial T}{\partial y}) \quad (13)$$

$$q_z=-k_z(\frac{\partial T}{\partial z}) \quad (14)$$

$$\frac{\partial q_x}{\partial x}+\frac{\partial q_y}{\partial y}+\frac{\partial q_z}{\partial z}+Q(x,y,z,t)=\rho C\frac{\partial T}{\partial t} \quad (15)$$

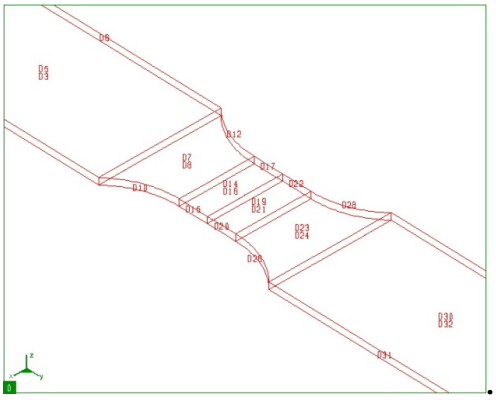

**Fig. 5.** Surfaces which exposed to air are represented by domains.

A domain V is divided into finite elements connected at nodes. In this section the relations for finite elements are expressed. Global equations for the domain can be assembled

from finite element equations using connectivity information.
For the interpolation of temperature inside a finite element shape, functions $N_i$ are used:

$$T = [N]\{T\} \quad (16)$$

$$[N] = [\, N_1 N_2 \ \dots \,] \quad (17)$$

$$\{T\} = \{\, T_1 T_2 \ \dots \,\} \quad (18)$$

Differentiation of temperature interpolation equations gives the following interpolation relation for temperature gradients. In this equation, {T} is a vector of temperature at nodes, [*N*] is a matrix of shape function, and [B] is the matrix for temperature gradient interpolation.
Using Galerkin method, the basic heat transfer equation can be rewritten as:

$$\begin{Bmatrix} \frac{\partial T}{\partial x} \\ \frac{\partial T}{\partial y} \\ \frac{\partial T}{\partial z} \end{Bmatrix} = \begin{bmatrix} \frac{\partial N_1}{\partial x} & \frac{\partial N_2}{\partial x} & \dots \\ \frac{\partial N_1}{\partial y} & \frac{\partial N_2}{\partial y} & \dots \\ \frac{\partial N_1}{\partial z} & \frac{\partial N_2}{\partial z} & \dots \end{bmatrix} \{T\} = [B]\{T\} \quad (19)$$

Applying the divergence theorem to the first three terms leads to obtaining Eq. (20).

$$\int_V \rho c \frac{\partial T}{\partial t} N_i dV - \int_V [\frac{\partial N_i}{\partial x} + \frac{\partial N_i}{\partial y} + \frac{\partial N_i}{\partial z}]\{q\} dV = \int_V Q N_i dV - \int_S \{q\}^T \{n\} N_i dS \quad (20)$$

$$\{q\}^T = [q_x q_y q_z] \quad (21)$$

$$\{n\}^T = [n_x n_y n_z] \quad (22)$$

where $\{n\}$ is an outer normal to the surface of the body. The FE software uses this equation by the insertion of boundary conditions mentioned in Section 3.3 to solve the heat transfer problem.

## 4. Results and discussion

Using the geometry, heat flux distribution model, and the mesh described above, the keyhole size and shape of the welded area were modeled in the software. Figure 6 shows the bead geometry operated with the power of 1700W, speed of 13.34mm/s, and focal position of -0.5 mm. Low speed resulted in considerably wider bead geometry than weld bead geometry operated at high speed, as shown in Figs. 6 and 7. Effect of welding speed can be also investigated from the macrographs.
With the decrease of the beam velocity, more heat was absorbed by the work piece and the rate of cooling was decreased. Low welding speed caused the heat source to stay longer on the surface and power or heat input per unit length of weld was increased; furthermore, the absorption of laser beam by base metal at low welding speeds was increased. As a result, the fusion and heat affected zone were more subjected to heat which caused them to become wider, as shown in Fig. 6.

### *4.1. Focal position*

The predicted fusion zones shown in Figs. 6 and 7 were considered to be in good agreement with the presented macrographs. As can be seen in Fig. 7, the focal beam position varied, while the other parameters including power and speed were kept constant to investigate the effect of focal position in the weld bead geometry. It is necessary for focal position to be positioned in such a way that the laser beam could produce the maximum penetration.
It can be seen in Fig. 8 that the variation of beam focal position by the amount of 0.5 mm from the surface toward below the surface did not develop significant changes in the bead geometry, which was in agreement with the experimental work. For focal position on the surface, fusion zone was extended up to the middle section of the work piece (circa 0.85 mm); but, for the focal position of -0.5 mm, the fusion zone was extended slightly below the half of the work piece height (circa 0.9 mm). When the laser focal point was located more closely to the center of the work piece, the penetration was slightly close to evaporate the melt surface and create the deeper keyhole [22]. For negative focal position, energy absorption increased in the weld pool due to multiple reflections.

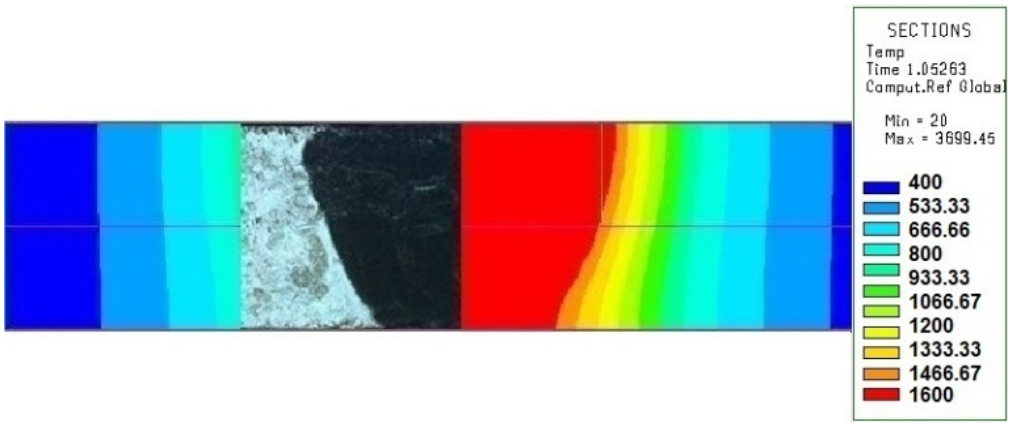


**Fig. 6.** Fusion boundry zone obtained from FEA in comparison to the experimental work. Power 1700 W, speed 13.34 $\frac{mm}{s}$ , and focal position -0.5 mm.

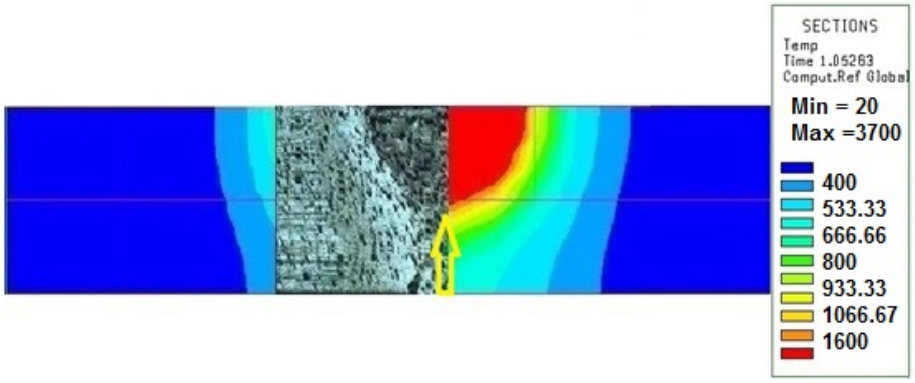


(a)

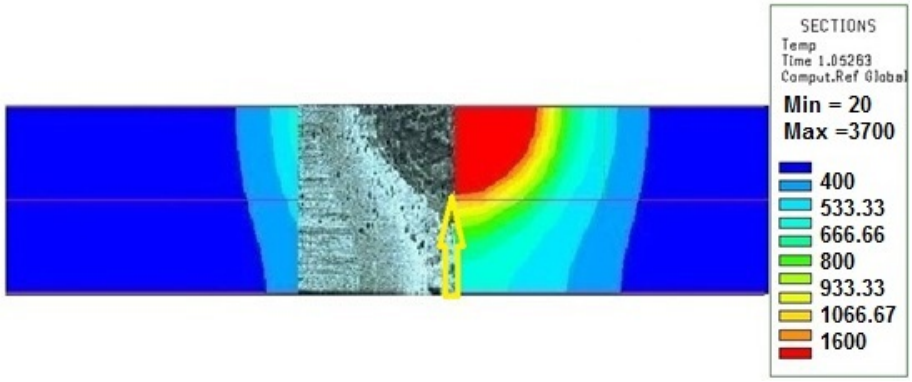


(b)

**Fig. 7.** Bead geometry from the experimental work in comparison to FEA results with two sets of welding parameters: a) Power of 1700 W, speed of 40$\frac{mm}{s}$ , and focal position of 0 (on the surface); b) Power of 1700 W, speed of 40$\frac{mm}{s}$ and focal position of -0.5 mm.

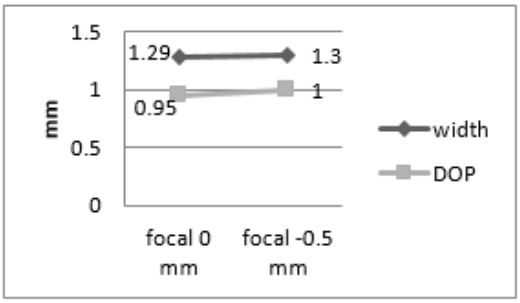


**Fig. 8.** Variation of DOP and width of the weld with focal position.

*4.2. Hardness*

Table 2 shows the average hardness of the fusion zone, HAZ, and base metal experimentally conducted on the surface of the work piece. Figure 9 shows hardness distribution on the surface obtained through FE method, which was in good agreement with the experimentally measured data. The hardness at the center of the weld pool was maximum due to the rapid cooling. The hardness dropped rapidly as getting distant from the fusion zone. Several hardness measurements were conducted by FE method at different speeds and the results are shown in Fig. 10.

**Table. 2.** Average hardness of FZ, HAZ and base metal.

| Base Metal | HAZ | Center line |
|---|---|---|
| 350 | 375 | 600 |

According to Fig. 10, it can be concluded that decreased speed caused the area with maximum hardness at the center of the weld to become wider; on the other hand, at low power, the area with maximum hardness was narrower. With lower laser speed, more heat input was transferred to the body; as a result, it took more time for the body to cool down. With decreasing cooling rates, maximum hardness was decreased. More difference in hardness between the weld pool and base metal was obtained at lower speeds.

*4. 3. Temperature distribution*

The temperature distribution of three marked areas on the surface of work piece which were stationed closely to the weld line can be seen in Fig. 11. This figure shows that there was a high temperature gradient adjacent to the centerline, while it dropped rapidly at farther areas from the center of the weld, due to the combination of fast cooling rates because of the convection and radiation losses and rapid rising of the temperature at the surface. The degree of the cooling rates in these areas is an important factor in determining different phases with various strength characteristics which occurs during welding. In addition to the welding parameters, maximum temperature also highly depends on reflectivity of the material and its capability to dissipate heat.

*4. 4. Heat distribution model*

To investigate the effect of heat source model on welding fusion zone geometry, two heat sources in welding, including conical 3D Gaussian and double ellipsoid Goldak distribution were applied, while other welding parameters were kept constant. As can be seen in Fig. 12, Gaussian model showed more precise results for simulating laser beam welding and calculating fusion zone dimensions.

By correctly adjusting Goldak parameters, only width of the weld was approximately close to the experimental results; however, Gaussian model could precisely simulate the depth and width of the penetration.

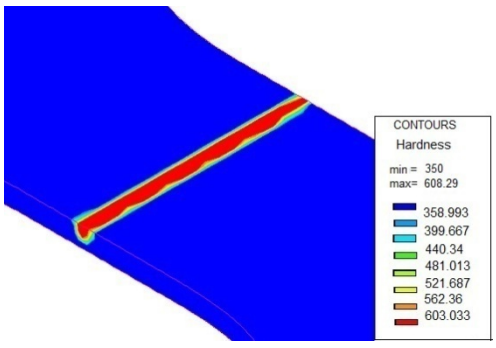


**Fig. 9.** Hardness distribution around the centerline of the weld.

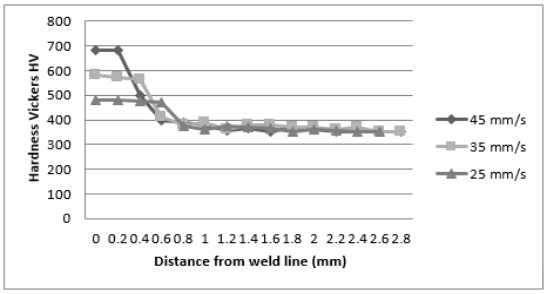


**Fig. 10.** Hardness distribution on the surface of the work piece.

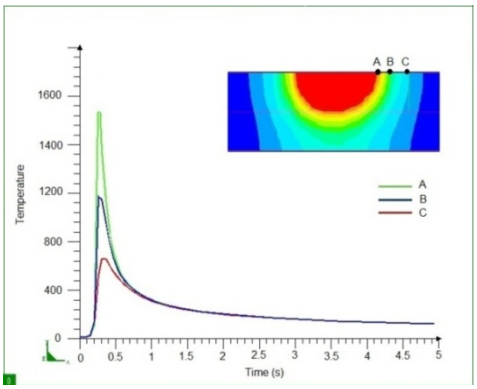


**Fig. 11.** Temperature history of different areas on the surface of the model.

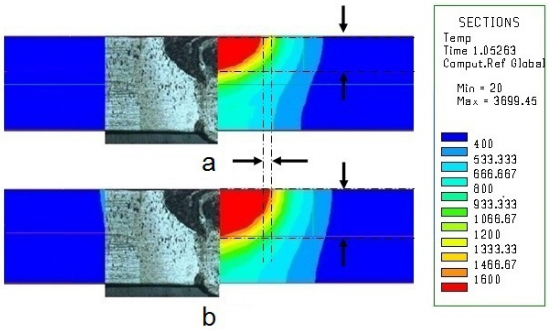


**Fig. 12.** Comparing fusion zone dimensions with the results obtained from using a) Goldak and b) Gaussian heat source.

## 5. Conclusions

A 3D finite element model was developed to simulate the laser welding process of butt joints to predict the temperature distribution and weld bead geometry. The finite element code SYSWELD was used to perform the analysis. Unlike most of the other three-dimensional simulations, the current study considered metallurgical transformation using temperature and phase-dependent properties. Several welding experiments were conducted to verify the FEA model. The predicted fusion zone was in good agreement with the provided macrograph. The conclusions can be summarized as follows:

- Variation of the focal position did not significantly alter penetration depth and weld bead geometry for the investigated material.
- The high velocity of the laser beam caused the weld bead to become smaller.
- The hardness at the center of the weld pool was maximum and higher laser speeds caused more difference in hardness between the weld pool and base metal.
- 3D conical Gaussian heat distribution can obtain better results than Goldak in laser beam welding with high depth to width ratio.

## References

[1] P. Sathiya, M. Y. AbdulJaleel, B. Katherasan and Shanmugarajan, "Optimization of laser butt welding parameters with multiple performance characteristics," *Optics & Laser Technology,* Vol. 43, No. 3, pp. 660-673, (2011).

[2] H. Wangand and M. D .Wei, "Tensile properties of LBW welds in Ti-6Al-4V alloy at evaluated temperatures below450$^{o}$C"*Materials Letters,* Vol. 57, No. 12, pp. 1815-1823, (2003).

[3] N. SivaShanmugam , G. Buvanashekaran and K. Sankaranarayanasamy, "Some studies on weld bead geometries for laser spot welding process using finite element analysis", *Materials and Design,* Vol. 34, No. 5, pp. 412-426, ( 2012).

[4] K. Y. Benyounis, A. G. Olabi and M. S. J. Hashmi, "Effect of laser welding parameters on the heat input and weld bead profile", *Journal of Materials Processing Technology,* Vol. 164-165, No. 4, pp. 978-985, (2005).

[5] Yi C. Liao and Y. Ming-Huei, "Effects of laser beam energy and incident angle on the pulse laser welding of stainless steel thin sheet", *Journal of Materials Processing Technology,* Vol. 190, No. 1, pp. 102-108, (2007).

[6] Du. Hanbin, Hu. Lunji, Liu. Jianhua and Hu. Xiyuan, "A study on the metal flow in full penetration laser beam welding for titanium alloy", *Computational Materials Science,* Vol. 29, No. 4, pp. 419-427, (2004).

[7] A. Aloraiera and S. Joshi, "Residual stresses in flux cored arc welding process in bead-on-plate specimens", *Materials Science and Engineering A*, Vol. 534, pp. 13-21, (2012).

[8] N. Siva Shanmugam and G. Buvanashekaran, "A transient finite element simulation of the temperature and bead profiles of T-joint laser welds", *Materials and Design*, Vol. 31, No. 9, pp. 4528-4542, (2010).

[9] LE. Lindgren,"Modeling for residual stresses and deformations due to welding-knowing what isn't necessary to know", *Math Model Weld Phenom*, Vol. 6, No. 7, pp. 791-518, (2001).

[10] P. Dong, "Residual stresses and distortion in welded structures", *A perspectivefor engineering applications. Sci Technol Weld Join,* Vol. 10, No. 10, pp. 89-98, (2005).

[11] M. Zain-ul-abdein and D. Nélias, "Finite element analysis of metallurgical phase transformations in AA 6056-T4 and their effects upon the residual stress and distortion states of a laser welded T-joint", *International Journal of Pressure Vessels and Piping,* Vol. 88, No. 1, pp. 45-56, (2011).

[12] J. B. Roelens, "Numerical simulation of some multipass submerged arc welding determination of residual stress and comparison with experimental measurements", *Welding in the world*, Vol. 33, No. 3, pp. 152-159, (1994).

[13] Y. V. L. N. Murthy, G. Venkata Rao and P. Krishnalyer, "Numerical simulation of welding and quenching processes using transient thermal and thermo-elasto-plastic formulations", *Computer & Structure,* Vol. 60, No. 1, pp. 131-154, (1996).

[14] S. Sarkani, V. Tritchkov and G. Michaelov, "An efficient approach for computing residual stresses in welded joints", *Finite Elen. Abal. Des.,* Vol. 35, No. 3, pp. 247-276, (2000).

[15] A. Khorramand, M. Ghoreishi, "$CO_2$ Laser Welding of a Ti6Al4V Alloy and the Effects of Laser Parameters on the Weld Geometry", *Lasers in Eng.,* Vol. 21, No. 7, pp. 135-148, (2011).

[16] J. Donachie, "Titanium: A Technical Guide. Metals Park", *ASM International*, (1988).

[17] S. A. Tsirkas. P. Papanikos and Th. Kermanidis, "Numerical simulation of the laser welding process in butt-joint specimens", *Journal of Materials Processing Technology*, Vol. 134, No. 1, pp. 59-69, (2003).

[18] K. N. Lankalapalli, J. F. Tu and M. Gatner, "A model for estimating penetration depth of laser welding processes", *Journal of Physics D*, Vol. 29, No. 27, pp. 197-214, (1996).

[19] K. Williams, "Development of laser welding theory with correlation to experimental welding data", *Laser Eng.* Vol. 8, No. 3, pp. 197-214, (1999).

[20] K. R. Balasubranian N. Shanmugam, G. Buvanashekaran and K. Sankaranarayanasamy, "Numerical and experimental investigation of laser beam welding of AISI 304 stainless steel sheet", *Advances in Production Engineering & Management,* Vol. 3, No. 2, pp. 93-105, (2008).

[21] A. Bappa, S. Arunanshu M. Souren and M. Dipten, "Finite element simulation of laser transmission welding of dissimilar materials between polyvinylidene fluoride and titanium", *International Journal of Engineering, Science and Technology,* Vol. 2, No. 4, pp. 176-186, (2010).

[22] M. Moradi and M. Ghoreishi, "An Investigation on the effect of pulsed Nd:YAG laser welding parameters of stainless steel", *Advanced Materials Research*, Vols. 383-390, No. 9, pp. 6247-625, (2012).